Chemical Engineering Journal 270 (2015) 450–458

Contents lists available at ScienceDirect

Chemical Engineering Journal

journal homepage: www.elsevier.com/locate/cej

Preparation of hierarchically porous diatomite/MFI-type zeolite composites and their performance for benzene adsorption: The effects of desilication

Wenbin Yu [a,b,c], Liangliang Deng [a,b,c], Peng Yuan [a,c,*], Dong Liu [a,c], Weiwei Yuan [a,b,c], Fanrong Chen [a,c]

[a] CAS Key Laboratory of Mineralogy and Metallogeny, Guangzhou Institute of Geochemistry, Chinese Academy of Sciences, Wushan, Guangzhou 510640, China
[b] University of Chinese Academy of Sciences, Beijing 100049, China
[c] Guangdong Provincial Key Laboratory of Mineral Physics and Materials, Wushan, Guangzhou 510640, China

HIGHLIGHTS

- Diatomite/zeolite composites prepared by vapor-phase transport and desilication.
- Desilication introduced mesoporosity and formed terminal silanol groups.
- The composites exhibited hierarchical porosity.
- The composites exhibited excellent benzene adsorption capacity.

ARTICLE INFO

Article history:
Received 11 December 2014
Received in revised form 7 February 2015
Accepted 16 February 2015
Available online 24 February 2015

Keywords:
Diatomite
Vapor-phase transport
MFI-type zeolite
Desilication
Hierarchical porosity
Benzene adsorption

ABSTRACT

Hierarchically porous diatomite/MFI-type zeolite composites were prepared by transforming the natural diatomaceous silica into MFI-type zeolite by a vapor-phase transport method, followed by a desilication treatment. The morphology and macroporosity of the diatomite were well preserved in the parent diatomite/MFI-type zeolite composite (Dt/Z). Treatment of Dt/Z by desilication in aqueous 0.2 M NaOH solution at 60 °C for 1 h resulted in a mesopore size distribution centered at approximately 7 nm, without significantly altering the macroporosity and microporosity of the resulting composite. Further desilication treatment (10 h) broadened the mesopore size distribution, whereas the macropores sourced from the diatomite support were significantly damaged and a fraction of the micropores was narrowed to approximately 0.49 nm. Under the optimal desilication condition (1 h), the desilication-treated Dt/Z sample (Dt/Z-A_{1h}) exhibited a higher adsorption capacity, better affinity, and faster adsorption kinetics toward benzene than the parent Dt/Z, as evaluated via a gravimetric method using an Intelligent Gravimetric Analyzer. The excellent benzene adsorption performance of Dt/Z-A_{1h} was attributed both to the increase in porosity and the formation of terminal silanol groups on the surface of newly developed pores after the desilication treatment.

1. Introduction

Volatile organic compounds (VOCs) are the most common air pollutants emitted from the chemical, petrochemical, pharmaceutical, building materials, and printing industries. Most VOCs are toxic or even carcinogenic (such as benzene) and are the main sources of photochemical reactions in the atmosphere, which lead to various environmental hazards [1,2]. Many technologies are available for VOCs control, such as adsorption [3], condensation [4], membrane separation [5], catalytic oxidation [6,7], and biological treatment [8], among which adsorption is the most applicable technology because of the flexibility of the system, low energy, and inexpensive operation costs [3,9].

Activated carbon has long been recognized as the most versatile adsorbent due to its low cost and excellent adsorption capacity [10]. However, several drawbacks are associated with its use in adsorption processes, such as hygroscopicity, pore clogging, and low thermal stability [11]. Hence, extensive efforts have been focused on finding alternative adsorbents [12–15]. MFI-type zeolites with low Al content or purely siliceous form (silicalite-1) have been proposed as potential VOCs adsorbents due to their high

* Corresponding author at: CAS Key Laboratory of Mineralogy and Metallogeny, Guangzhou Institute of Geochemistry, Chinese Academy of Sciences, Wushan, Guangzhou 510640, China. Tel./fax: +86 20 85290341.
E-mail address: yuanpeng@gig.ac.cn (P. Yuan).

http://dx.doi.org/10.1016/j.cej.2015.02.065
1385-8947/

hydrophobicity/organophilicity, large surface area, and superior thermal stability [16,17]. However, these zeolites possess only micropore channels [18], resulting in both relatively slow mass transport and a high price, which is caused mainly by the need to use expensive organic templates and inorganic sources during the preparation process. These limitations have greatly hindered their use in adsorption processes.

Diatomite, also known as diatomaceous earth or kieselguhr, is a fine-grained, low-density biogenic sediment, consisting of amorphous hydrated silica ($SiO_2 \cdot nH_2O$) derived from opalescent frustules of diatoms [19,20]. Diatoms are unicellular algae, microscopic plants that existed during tertiary and quaternary periods. One unique feature of diatoms is their highly developed porosity and, in particularly, a macroporous structure with pore sizes ranging from the nanometric to micrometric domains [21–24]. Diatomite is relatively inexpensive because diatomaceous silica is the most abundant form of silica on Earth, and there are significant diatomite reserves worldwide. In previous investigations, diatomite has been used as a support to prepare diatomite/zeolite composites (supported zeolites) by offering two major advantages [25–27]: its macroporous structure can improve the efficiency of mass-transport and diffusion processes; and being made of silica, diatomite can act as an inexpensive inorganic silicon source for zeolite growth. For example, Anderson et al. [25] prepared a diatomite/ZSM-5 composite through the hydrothermal treatment of an ultrasonic seeded diatomite in a clear synthesis solution containing an adscititious silicon source and observed a high diffusion rate of water; Wang et al. [26] prepared a hierarchically structured diatomite/MFI-type zeolite composite through a more economical and effective vapor-phase transport (VPT) method, in which the diatomaceous silica was partially transformed into zeolite. Although the overall diffusion performance of the aforementioned composites was improved due to the introduction of macroporosity by the diatomite support, the intracrystalline diffusion rate of diatomite-coated zeolite crystals may only yield a minor improvement compared to pure (unsupported) zeolites. Therefore, a possible strategy to further improve the diffusion performance of diatomite/zeolite composites is to enhance the intracrystalline diffusion rate of diatomite-coated zeolite crystals.

Post-synthesis treatment of parent zeolites can increase the porosity due to the appearance of defect sites in the zeolite framework. Thus, it can improve the gas transport characteristics of zeolites. Well-known post-treatments include steaming at relatively high temperatures [28], acid leaching [29], and, more recently, alkaline treatment [30]. Alkaline treatment selectively removes silicon from the zeolite framework, whereas steaming and acid leaching lead to dealumination. Dealumination is mainly used to stabilize the zeolite structure or to create Lewis acidity, and increase in porosity is rather limited [31]. The desilication treatment is a more efficient method to induce mesoporosity in zeolite crystals [32,33]. As inferred in the above-mentioned studies, it would be of interest to combine the coating of zeolite crystals on the surface of diatomite with the desilication treatment to achieve an improvement on the mass-transport and diffusion efficiency. However, to the best of our knowledge, related studies have not been reported to date.

In this study, a diatomite/MFI-type zeolite composite was prepared through a VPT process, thus introducing macroporosity in the zeolite material. Then, the composite was treated by desilication in an alkaline medium to create mesopores in the zeolite crystals coated on the surface of the diatomite. Treatment of the parent diatomite/MFI-type zeolite composite in aqueous 0.2 M NaOH solution at 60 °C for 1 h resulted in a mesopore size distribution centered at approximately 7 nm, without significantly altering the macroporosity and microporosity of the resulting composite. Thus, the desilication-treated diatomite/MFI-type zeolite composite exhibited a special trimodal porosity: macroporosity sourcing from the diatomite support, mesoporosity created by desilication treatment, and microporosity of MFI-type zeolite. This is a significant optimization in the pore structure compared with the previous reported diatomite [25–27] or other substrate (e.g., porous stainless steel, porous glass or solid foam monoliths) supported zeolites [34–36], which could be helpful for the improvement of the adsorption performance of such materials. Benzene was used as a model pollutant to evaluate the adsorption performance of the resulting composites for VOC. Benzene was specifically chosen, because it is released from multiple sources (e.g., petrochemical plants, petroleum tanks, coke ovens, printing office, and Chinese-style cooking) and has been proven to be carcinogenic [1,8]. The benzene static adsorption capacity and adsorption kinetics on the resulting composites were studied based on a gravimetric method using an Intelligent Gravimetric Analyzer (IGA), which have rarely been reported in previous studies concerning the similar diatomite/zeolite composites [25–27]. The influences of desilication on the structure and the benzene adsorption performance of the prepared composites were investigated.

2. Experimental

2.1. Reagents and materials

Tetraethoxysilane (TEOS, 99%) and diallyldimethylammonium chloride (PDDA, 20 wt% in the water) were purchased from Aldrich. Tetrapropylammonium hydroxide (TPAOH, 25 wt% in the water) was obtained from Zhejiang Kente Chemical Co., Ltd. Sodium hydroxide pellets (AR Grade) were purchased from Nanjing Chemical Reagent Co., Ltd. All reagents were used as received without any further purification. Distilled water was used in all experiments. The raw diatomite was obtained from Qingshanyuan diatomite Co., Ltd. (Jilin provinces, China), and purified via a sedimentation method [37]. The chemical composition (wt%) of the purified diatomite (hereafter denoted as Dt) is as follows: SiO_2, 85.76; Al_2O_3, 5.60; Fe_2O_3, 1.74; K_2O, 0.99; CaO, 0.33; MgO, 0.01; Na_2O, 0.20; TiO_2, 0.26; ignition loss, 4.64.

2.2. Preparation of the diatomite/MFI-type zeolite composite

The diatomite/MFI-type zeolite composite (Dt/Z) was prepared via a VPT process as previously reported by Wang et al. [26]. The aqueous suspension of 80-nm silicalite-1 seeds (Sil-1) was prepared following a procedure described in the literature [38]: a synthesis mixture with a molar ratio of $25SiO_2$:9TPAOH:$480H_2O$:100EtOH was heat-treated in a polypropylene bottle under reflux in a silicone oil bath at 100 °C for 48 h. TPAOH acted as template; here, the silica source was TEOS, and EtOH (Ethanol) was the hydrolysis product of TEOS. A layer-by-layer electrostatic assembly technique was used to perform the seeding process [39]. Typically, 0.5 g of diatomite powder was immersed in 25 mL of 5 wt% PDDA solution for 30 min, and then, the solid phase in the resultant mixture was centrifuged (4000 rpm for 5 min) and washed four times with distilled water to remove the excess polyelectrolyte. Next, the modified sample was added to 25 mL of pH 9.5, 1.5 wt% Sil-1 suspension and left in contact with this solution for 30 min. The excess of Sil-1 was removed by washing four times with 0.10 M ammonia solution and centrifugation at 4000 rpm for 5 min. This layer-by-layer seeding procedure was performed only once, producing Sil-1 monolayer-seeded diatomite samples. Subsequently, 0.5 g of the seeded sample was placed on a porous Teflon board, that was placed horizontally in the middle of a Teflon-lined stainless steel autoclave and 5 g of a liquid mixture of ethylenediamine, triethylamine, and H_2O with a molar ratio of 2:9:6 was injected into the

bottom of the autoclave. The autoclave was then placed in an oven at 180 °C and heated for 10 days, ensuring the maximal transformation of diatomaceous silica to zeolite [26]. Afterward, the as-synthesized sample was calcined at 550 °C in air for 6 h (heating rate of 5 °C min^{-1}) to remove the organic template. The resultant sample was denoted as Dt/Z.

2.3. Desilication treatment

The desilication treatment of the Dt/Z composite was performed in NaOH solution at 60 °C. Typically, 0.5 g of Dt/Z composite was vigorously stirred in 10 ml of 0.2 M NaOH solution for different periods of time (1–10 h). The resulting samples were washed thoroughly with distilled water before being dried at 80 °C overnight. The obtained products were denoted as Dt/Z-A_{nh}, where n indicates the desilication treatment time in hours.

2.4. Characterization methods

The XRD patterns were recorded using a Bruker D8 Advance diffractometer with Ni filter and CuKα radiation (λ = 0.154 nm), a generator voltage of 40 kV and a current of 40 mA. The scan rate was 3° (2θ)/min. N_2 adsorption–desorption isotherms were measured with a Micromeritics ASAP2020 system at liquid-nitrogen temperature. Samples were outgassed at 350 °C for 12 h before measurement. The total surface area of the sample, S_{BET}, was calculated from the nitrogen adsorption data using the multiple-point Brunauer–Emmett–Teller (BET) method [40], and the total pore volume, V_{total}, was evaluated based on nitrogen uptake at a relative pressure of approximately 0.99. The micropore surface area, S_{micro}, and micropore volume, V_{micro}, were derived from the t-plot method [41]. The mesopore size distribution was calculated according to the Barrett–Joyner–Halenda (BJH) model [42], and the micropore size distribution was determined using the Saito–Foley (SF) model for cylindrical pore geometry [43] applied to the adsorption branch of the isotherm. SEM micrographs were acquired using a ZEISS SUPER 55 field emission scanning electron microscope. Diffuse reflectance Fourier transform infrared (DRIFT) spectra were obtained using the Praying Mantis™ diffuse reflection accessory of a Bruker Vertex-70 Fourier transform infrared spectrometer at room temperature. The spectra were collected over the range of 600–4000 cm^{-1} with 64 scans at a resolution of 2 cm^{-1} using KBr as the background.

2.5. Benzene adsorption tests

The benzene adsorption performance of the obtained samples was evaluated using an IGA (IGA-002, Hiden Isochema Instrument) with a sensitivity of 0.1 μg. This apparatus is an ultrahigh vacuum system, that allows isotherms and the corresponding kinetics of adsorption to be determined by setting pressure steps [44]. Before the measurements, the adsorbent sample (approximately 50 mg for each run) was outgassed at 350 °C for 8 h under vacuum conditions to remove the excess water and impurities absorbed in the pores. During sorption measurements, the pressure was altered with the set pressure points and the mass uptake was measured in real time using a computer algorithm. After equilibrium was established for a desired pressure value, the vapor pressure was increased to the next set pressure value, and the subsequent uptake was measured until equilibrium was reestablished. The increase in weight due to adsorption for each pressure step was used to calculate the kinetic parameters for adsorption using an appropriate kinetic model [45]. The adsorption experiments were carried out at a temperature of 25 °C.

3. Results and discussion

3.1. Characterization of the Dt support and Dt/Z composite

The XRD pattern of Dt (Fig. 1a) revealed the main phase of non-crystalline opal-A with a characteristic broad peak centered at 21.8° (2θ). Quartz impurity was also observed in the Dt sample (Fig. 1a), and its content (wt%) was semi-quantitatively determined as approximately 4%. The newly appeared characteristic reflections of the MFI-structured zeolite at 8.0°, 8.8°, 23.3°, 24.0°, and 24.4° (2θ) [46] in the XRD pattern (Fig. 1b) indicated the presence of an MFI-type zeolite in the Dt/Z composite.

As indicated by the SEM image (Fig. 2a), the dominant diatom of the Dt sample, which is classified in the genus *Coscinodiscus* Ehrenberg (*Centrales*), is disk-shaped and has a highly developed macroporous structure. The diatom frustules are relatively uniform in diameter (20–40 μm) and thickness (1.2–1.8 μm; SEM images not shown). The surface of the diatom frustule appeared to be extremely smooth when observed at a high magnification (Fig. 2b). Fig. 2c shows the SEM image of the Dt/Z composite, which illustrates that, the original disk morphology and the macroporous structure of diatomite are both preserved after VPT treatment of the Sil-1 seeded diatomite sample. As shown in Fig. 2d, the surface of the diatom frustule is completely coated with a layer of MFI-type zeolite crystals, whose morphology was converted to quadrate crystals from the original sphere of Sil-1 (Supplementary Fig. S1). The average size of the zeolite crystals increased from approximately 80 nm to 200 nm. Because no additional silica source was added to the reaction system, the diatomaceous silica must have acted as a silica source for the growth of the zeolite crystal coating on the surface of the diatom frustules.

The N_2 adsorption–desorption isotherm of Dt is characterized as a type II isotherm with an H3 hysteresis loop (Fig. 3a) according to the IUPAC classification [47]. The hysteresis is associated with the filling and emptying of the mesopores by capillary condensation, indicating the existence of mesopores in the Dt. In addition, the sharp increase in the amount of N_2 adsorbed near the relative pressure of 1 corresponds to the adsorption by macropores [48,49]. The type IV N_2 isotherm of the Dt/Z sample (Fig. 3b) is indicative of the

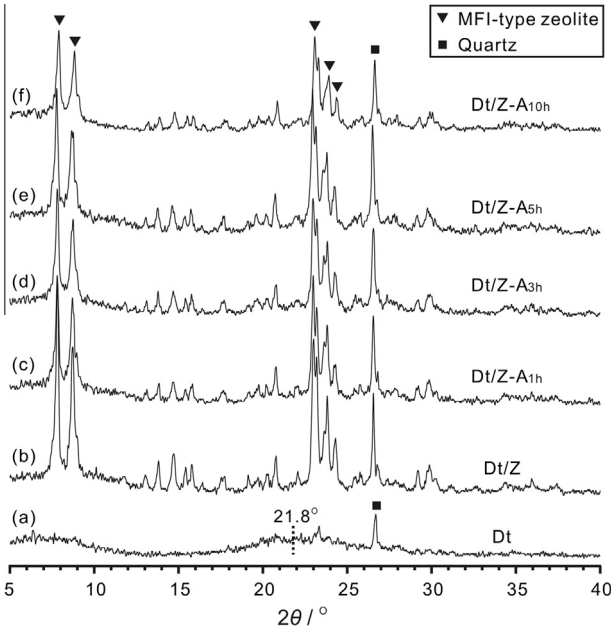

Fig. 1. XRD patterns of (a) Dt, (b) Dt/Z, (c) Dt/Z-A_{1h}, (d) Dt/Z-A_{3h}, (e) Dt/Z-A_{5h}, and (f) Dt/Z-A_{10h}.

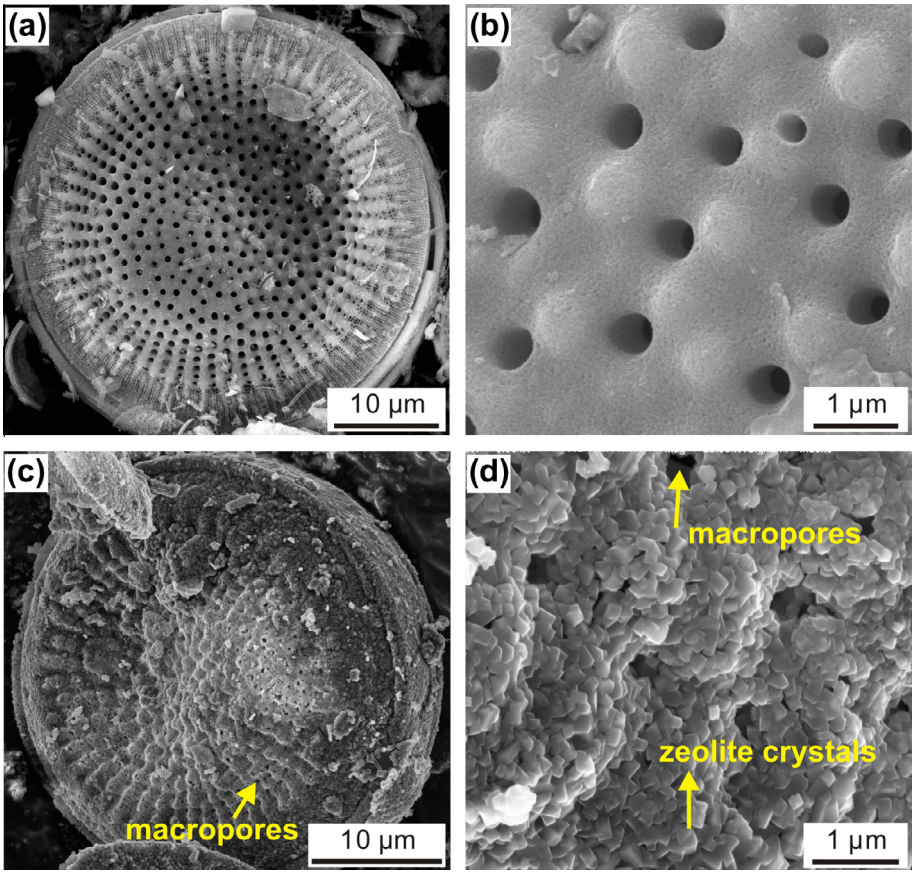

Fig. 2. SEM images of (a and b) Dt and (c and d) Dt/Z.

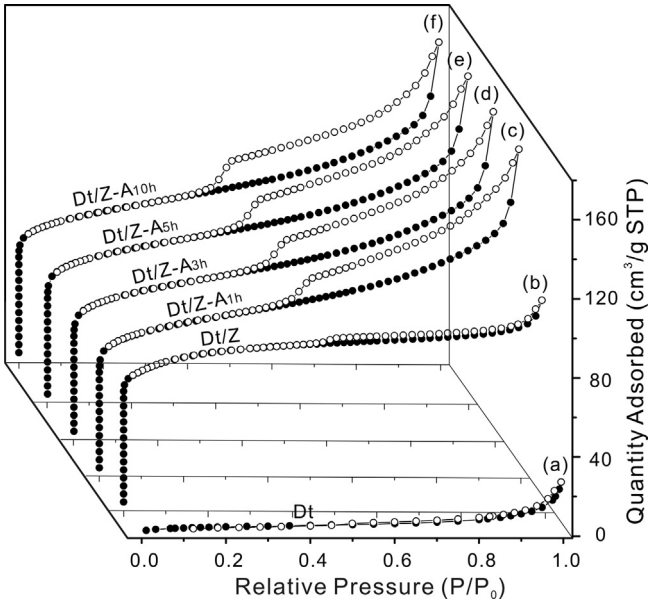

Fig. 3. N_2 adsorption–desorption isotherms of (a) Dt, (b) Dt/Z, (c) Dt/Z-A_{1h}, (d) Dt/Z-A_{3h}, (e) Dt/Z-A_{5h}, and (f) Dt/Z-A_{10h}.

newly generated porosity in the material, the steep rise at low relative pressures corresponds to the filling of zeolitic micropores, and the hysteresis loop implies the intercrystalline mesopores space. The S_{BET} and S_{micro} value of Dt/Z are 295.7 and 234.9 m^2/g, respectively, which are significantly larger than those of the Dt support

Table 1
Textural properties of Dt, Dt/Z, and the desilication-treated samples (Dt/Z-A_{nh}).

Sample	S_{BET} (m^2/g)	S_{micro} (m^2/g)	S_{meso}[a] (m^2/g)	V_{total} (cm^3/g)	V_{micro} (cm^3/g)	V_{meso}[a] (cm^3/g)
Dt	16.8	8.7	6.7	0.042	0.004	0.019
Dt/Z	295.7	234.9	8.7	0.164	0.095	0.016
Dt/Z-A_{1h}	286.9	190.2	37.1	0.255	0.077	0.061
Dt/Z-A_{3h}	285.4	188.3	36.8	0.256	0.076	0.060
Dt/Z-A_{5h}	288.9	192.7	35.9	0.255	0.078	0.059
Dt/Z-A_{10h}	280.4	182.7	35.5	0.249	0.074	0.058
Sil-1	509.8	397.4	48.3	0.720	0.155	0.188

[a] BJH cumulative adsorption surface area and volume of pores between 2.0 and 50.0 nm.

(Table 1). This indicated that the majority of the surface area of Dt/Z is due to the micropores, and that the contribution from the mesopores is relatively low. The BJH cumulative adsorption surface area of pores between 2.0 and 50.0 nm, S_{meso}, is only 6.7 m^2/g (Table 1). The content of MFI-type zeolite in the Dt/Z composite was 58.7%, calculated from the micropore volume (Table 1) by using the equation $W_z = [V_{micro}(Dt/Z) - V_{micro}(Dt)]/V_{micro}(Sil\text{-}1)$ [26], where W_z is the zeolite content.

3.2. Effects of desilication on the structure of Dt/Z-A_{nh}

All of the desilication-treated samples exhibited XRD patterns similar to that of the Dt/Z sample (Fig. 1), indicating that the lattice structure of the MFI-type zeolite was still preserved. The intensity of the characteristic peaks of MFI-structured zeolite decreased with the desilication treatment time, indicating the loss of crystallinity upon desilication treatment. This result is due to the

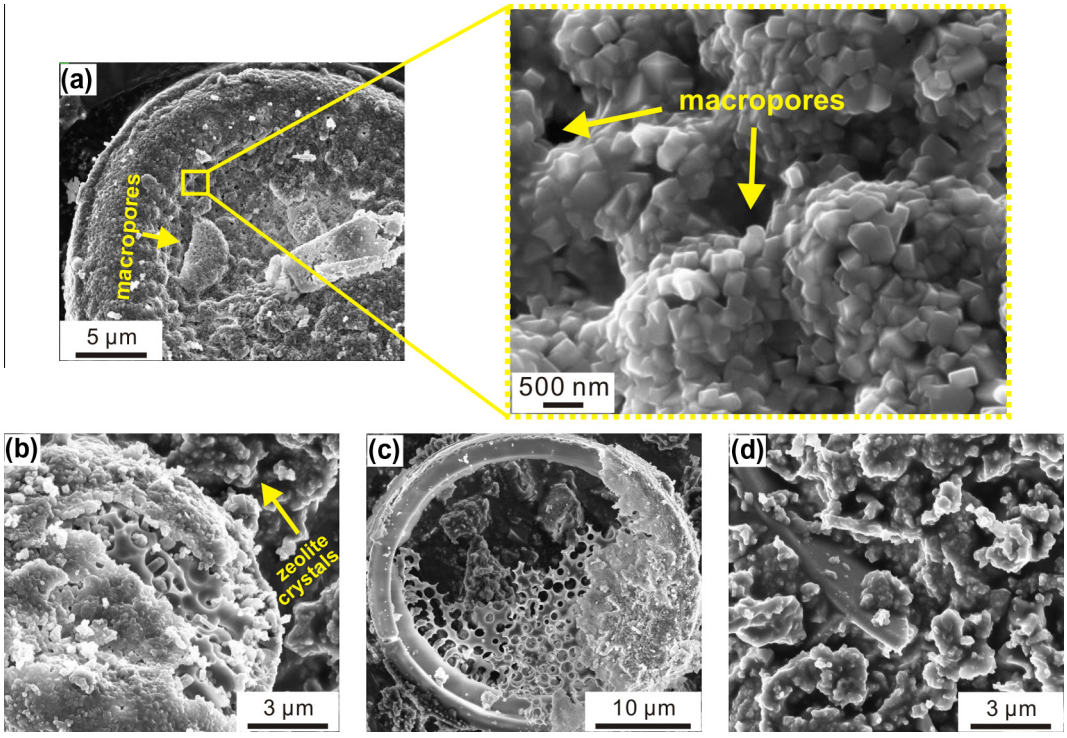

Fig. 4. SEM images of (a) Dt/Z-A_{1h}, (b) Dt/Z-A_{3h}, (c) Dt/Z-A_{5h}, and (d) Dt/Z-A_{10h}.

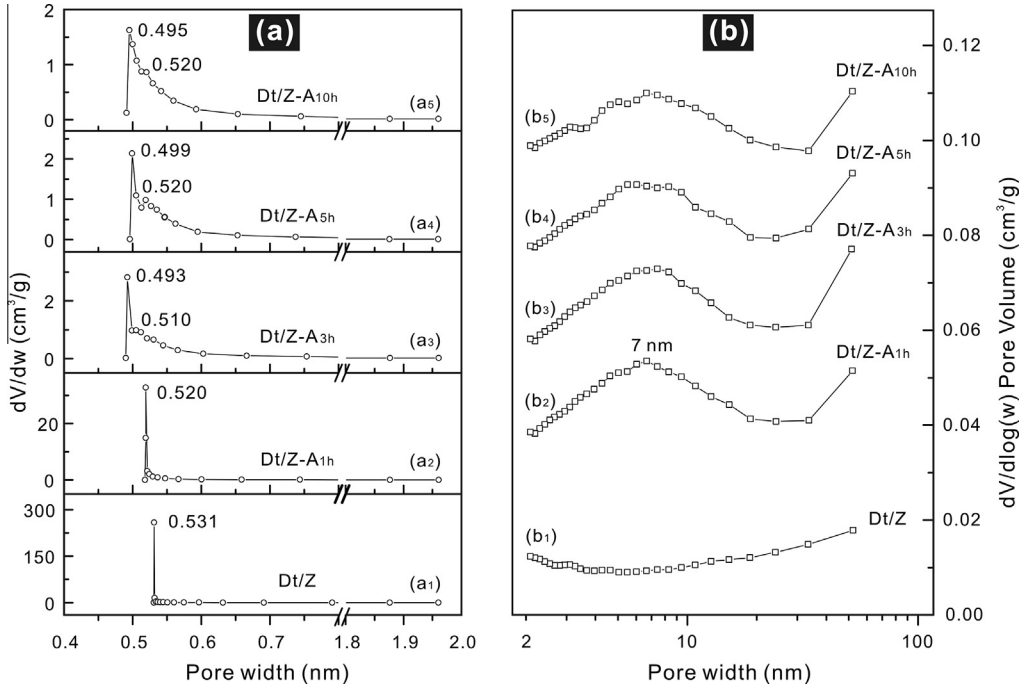

Fig. 5. (a) SF micropore size distributions of (a_1) Dt/Z, (a_2) Dt/Z-A_{1h}, (a_3) Dt/Z-A_{3h}, (a_4) Dt/Z-A_{5h}, and (a_5) Dt/Z-A_{10h}; (b) BJH mesopore size distributions (adsorption branch) of (b_1) Dt/Z, (b_2) Dt/Z-A_{1h}, (b_3) Dt/Z-A_{3h}, (b_4) Dt/Z-A_{5h}, and (b_5) Dt/Z-A_{10h}. (b_3), (b_4), and (b_5) are shifted 0.02, 0.04, and, 0.06 cm^3/g upward, respectively, for clarity.

removal of Si from the framework and the creation of additional mesopores in the MFI-type zeolite crystals [30,50].

The overall morphological and macroporous changes of Dt/Z during the desilication treatment were revealed by SEM. Fig. 4 shows the SEM images acquired after the desilication treatment of Dt/Z for the time range of 1–10 h. No obvious change in the disk morphology and macroporous structure of Dt/Z was observed for the 1 h treatment (Fig. 4a). Upon further desilication treatment (3 h), the diatom frustules began to dissolve and the zeolite coating became incomplete (Fig. 4b). Some zeolite crystals that were dropped from the diatom frustules can be found in the SEM image of Dt/Z-A_{3h} (Fig. 4b). After 5 h of desilication treatment, the disk morphology and macroporous structure of diatomite were significantly damaged (Fig. 4c and d). All of the diatom frustules were

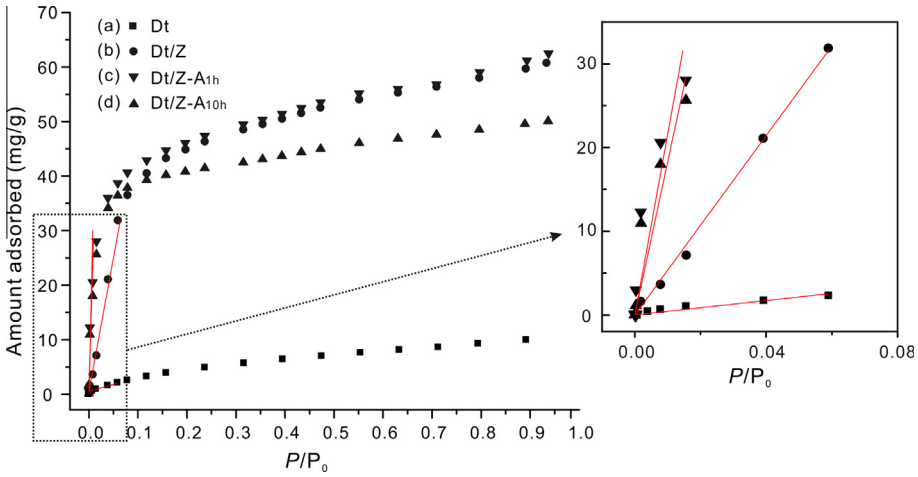

Fig. 6. Benzene adsorption isotherms of (a) Dt, (b) Dt/Z, (c) Dt/Z-A_{1h}, and (d) Dt/Z-A_{10h} (red solid lines for simulated based on Henry's law equation). (For interpretation of the references to color in this figure legend, the reader is referred to the web version of this article.)

dissolved, and the zeolite crystals congregated together in the Dt/Z-A_{10h} sample (Fig. 4d).

The mesopore and micropore changes due to the desilication treatment were studied by N_2 adsorption measurements. Upon desilication treatment, the development of a distinct hysteresis loop in the N_2 adsorption–desorption isotherm was observed (Fig. 3c–f), indicating the generation of new mesopores in the desilication-treated sample. The steep increase at low relative pressures still corresponded to the filling of zeolitic micropores (Fig. 3c–f). The N_2 adsorption–desorption isotherm of Dt/Z-A_{1h} exhibited a more distinct hysteresis loop (Fig. 3c) than that of Dt/Z, suggesting that a substantial amount of mesopores formed after the desilication treatment for 1 h. A further increase in the treatment time did not significantly change the entire profile of the isotherms as shown in Fig. 3.

Fig. 5a shows the SF micropore size distributions of the desilication-treated samples. A narrow peak at 0.531 nm, which corresponded to the mean micropore diameter of the MFI-type zeolite channels [18], was observed in the micropore size distribution of Dt/Z (Fig. 5a_1). Desilication treatment for 1 h broadened the micropore size distribution of Dt/Z-A_{1h}, and the mean micropore diameter decreased to 0.520 nm (Fig. 5a_2). When the desilication treatment time reached 3 h, a micropore size distribution centered at 0.493 nm was observed (Fig. 5a_3), indicating that desilication created new micropores that were significantly narrower than those of the parent zeolite. These narrower micropores were derived from a fraction of the micropore channels of the MFI-type zeolite that rearranged upon the desilication treatment. As illustrated by Fig. 5a_4 and a_5, the micropore size distributions below 0.5 nm broadened with the increase in desilication treatment time, indicating that more of the narrower micropores were created. These results were in good agreement with previous observations of ZSM-5 zeolite [51].

Fig. 5b shows the BJH mesopore size distributions of the desilication-treated samples. A relatively narrow mesopore distribution centered at approximately 7 nm was observed after 1 h desilication treatment (Fig. 5b_2). The S_{meso} and V_{meso} value of Dt/Z-A_{1h} are 37.1 m^2/g and 0.061 cm^3/g, respectively, which are approximately 3 times greater than those of Dt/Z, whereas the S_{mico} and V_{mico} value decreased by only approximately 20% (Table 1). A longer treatment time shows a gradual broadening of the mesopore size distributions (Fig. 5b), and the S_{meso} value of the desilication-treated sample exhibits a slight decrease after 3 h of desilication treatment (Table 1). Based on the SEM and the pore (micropore and mesopore) size distribution results, the optimal desilication time for introducing mesopores while keeping the macroporous and microporous structure of Dt/Z was 1 h.

Table 2
Equilibrium adsorption capacities q^e (mg/g) and Henry modal parameters of benzene on Dt, Dt/Z, Dt/Z-A_{1h} and Dt/Z-A_{10h}.

Samples	Equilibrium adsorption capacities q^e (mg/g)	Model parameters	
		Henry constants H (10^3 mg/g)	R^2
Dt	11.1	0.043	0.954
Dt/Z	60.8	0.536	0.998
Dt/Z-A_{1h}	62.5	2.019	0.941
Dt/Z-A_{10h}	50.1	1.830	0.951

3.3. Effects of desilication on the benzene adsorption performance of Dt/Z-A_{nh}

The desilication-treated diatomite/MFI-type zeolite composites Dt/Z-A_{1h} with trimodal porosity and Dt/Z-A_{10h} with bimodal porosity were adopted here as representative samples to estimate their benzene adsorption performance when compared with Dt/Z and Dt. Fig. 6 presents the adsorption isotherms of benzene on Dt, Dt/Z, Dt/Z-A_{1h} and Dt/Z-A_{10h}. The Henry's law [52,53] was used to fit the adsorption data in the very-low-pressure region (the area in the dashed rectangle in Fig. 6), where interaction between adsorbed molecules could be neglected and only interactions between adsorbed molecules and the adsorbent surface remained [53]. The Henry's law is described by the following equation:

$$q = H\frac{p}{p_0} \quad (1)$$

where q (mg/g) is the amount of absorbed benzene at the relative pressure p/p_0 and H (10^3 mg/g) is the Henry constant, which reflects the adsorption affinity between a benzene molecule and the adopted sample surface. As shown in Table 2, the H values for all Dt/Z composites were significantly larger than that for Dt. This result was due to the microporosity of the Dt/Z samples, and the fact that the micropores had a high adsorption energy [54]. The H values for Dt/Z-A_{1h} and Dt/Z-A_{10h} were significantly larger than that for Dt/Z (Table 2), indicating that the desilication treatment strengthened the adsorption affinity between the benzene molecule and the surface of the Dt/Z composites.

As shown by the results of DRIFT spectra (Supplementary Fig. S2), the desilication treatment of Dt/Z resulted in an increase

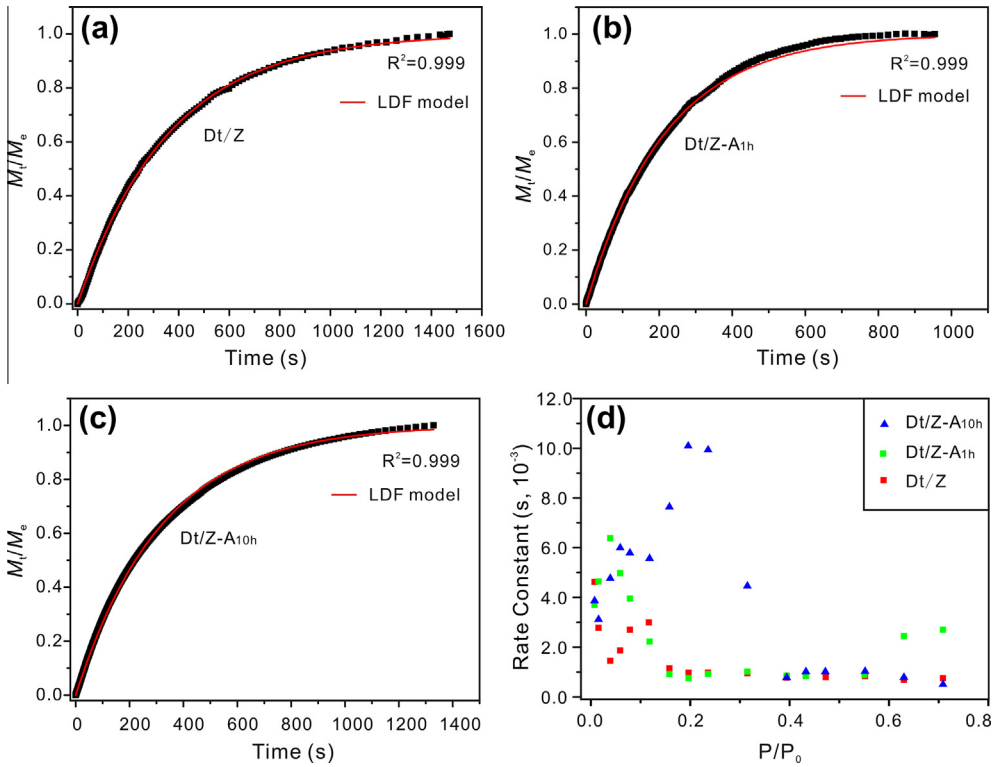

Fig. 7. Variation of M_t/M_e versus time for benzene adsorption on (a) Dt (p/p_0 = 0.00786–0.0156), (b) Dt/Z-A_{1h} (p/p_0 = 0.00781–0.0156), and (c) Dt/Z-A_{10h} (p/p_0 = 0.00778–0.0156); (d) variation of rate constants with relative pressure on Dt, Dt/Z-A_{1h}, and Dt/Z-A_{10h}.

in the relative intensity of the band at 3745 cm^{-1}, which was associated with terminal silanol groups of MFI-type zeolite [55]. This result indicated that terminal silanol groups were formed on the newly developed pore surface after the desilication treatment. After benzene adsorption, the intensity of the band at 3745 cm^{-1} decreased and, accordingly, a new band at 3652 cm^{-1} became well resolved (Supplementary Fig. S2). This new band is assigned to the stretching vibrations of perturbed terminal silanol groups formed by hydrogen bonding to benzene [56]. Thus, the improved adsorption affinity between the Dt/Z composites and a benzene molecule, due to the desilication, can be explained by the formation of terminal silanol groups on the newly developed pore surface of the desilication-treated samples, which provided adsorption sites and had a high affinity to benzene molecule through hydrogen bonding.

The equilibrium adsorption capacity of benzene (q^e) for Dt/Z is 60.8 mg/g, which is significantly larger than that for Dt (Table 2). This result is attributed to the adsorption of benzene by MFI-type zeolite coated on the surface of Dt. MFI-type zeolite possess micropore channels in the range of 0.51–0.57 nm (sinusoidal channels with 0.54 nm circular cross sections interconnected with straight channels with 0.51 nm × 0.57 nm elliptical cross sections) [18]. It adsorbs benzene with molecular diameter of 0.5 nm [57,58]. Dt/Z-A_{1h} exhibited a larger q^e value than Dt/Z (Table 2). This increase in q^e value was due to the formation of mesopores in Dt/Z-A_{1h} (Fig. 5b_2) after 1 h of desilication treatment, resulting in increase in both the V_{meso} and V_{total} values (Table 1). Moreover, the micropores of Dt/Z-A_{1h} can also adsorb benzene molecule, because the micropores size of Dt/Z-A_{1h} is larger than the molecular diameter of benzene (Fig. 5a_2). This result was in accordance with the fact that the static VOC adsorption capacity is proportional to the total pore volume [59]. However, Dt/Z-A_{10h} exhibited a lower q^e value than Dt/Z-A_{1h} (Table 2), although the V_{micro}, V_{meso}, and V_{total} of Dt/Z-A_{10h} are comparable to those of Dt/Z-A_{10h} (Table 1). This result was due to the narrowing of a fraction of the micropores in Dt/Z-A_{10h}, as already indicated by the micropore size distribution (Fig. 5a_5). The narrowed micropores with a pore size of 0.493 nm (Fig. 5a_5) cannot adsorb molecules as large as benzene.

Adsorption kinetics is of fundamental importance in applications of adsorbents in actual situations [60]. The mass relaxation curves obtained by pressure increment could be used to calculate the adsorption kinetics [45]. The linear driving force (LDF) model, which was followed for substantial parts of the adsorption isotherms of benzene on microporous material [60] and mesoporous silica material [44], was used to fit the mass relaxation curve of the adopted samples. The LDF model for adsorption is described by the following equation:

$$\frac{M_t}{M_e} = 1 - e^{-kt} \quad (2)$$

where M_t is the uptake at time t, M_e is the equilibrium uptake for the given pressure increment ($M_t = M_e$ at equilibrium), and k is the rate constant [60].

Fig. 7a–c display the typical mass relaxation curves of M_t/M_e versus time for the adsorption of benzene on Dt/Z, Dt/Z-A_1, and Dt/Z-A_{10}, respectively, and the corresponding profiles were fitted using the LDF model. All three graphs show that the adsorption kinetics correspond well with the LDF model, with a correlation coefficient (R^2) ⩾ 0.998. The adsorption kinetics follow the LDF model over the relative pressure range of 0–0.709, and the detailed simulation results are provided in Supplementary Table S1. This result suggests that benzene diffusion through a barrier is the rate-determining step [45]. The barrier may be caused by the molecular being similar to the micropore size of the MFI-type zeolite or by a surface diffusion resistance.

A comparison of the LDF adsorption rate constant of benzene with relative pressure on Dt/Z, Dt/Z-A_1, and Dt/Z-A_{10} is shown in Fig. 7d. In the initial uptake region, the adsorption rate constants for Dt/Z-A_{1h} and Dt/Z-A_{10h} are significantly larger than those for Dt/Z (Fig. 7d). This observation can be attributed to (i) the mesopores created by desilication allowing for high accessibility during

adsorption; (ii) the terminal silanol formed after desilication treatment having a high affinity for the benzene molecule. For all samples, the adsorption rate constant initially decrease to a plateau when the relative pressure is larger than 0.4. This decrease in rate constants can be attributed to the development of clusters of molecular benzene in the micropores of the adsorbents [61]. The increase in rate constants for Dt/Z-A_{1h}, when the relative pressure is greater than 0.6 is likely related to the mass transport of macropores. This comparison between the adsorption rate constant of Dt/Z and that of the desilication-treated samples indicated that a desilication treatment improved the diffusion of Dt/Z composites, resulting in higher adsorption efficiency.

4. Conclusions

Hierarchically porous diatomite/MFI-type zeolite composites were prepared. A diatomite/MFI-type zeolite composite (Dt/Z) was prepared through a vapor-phase transport method, followed by a desilication treatment to increase the porosity of Dt/Z. The results have proven that optimization of the desilication treatment of the parent Dt/Z leads to an increased mesoporosity and preserved macroporosity and microporosity. The desilication-treated sample exhibited a higher adsorption capacity and better affinity, as well as faster adsorption kinetics toward benzene than the parent Dt/Z, due to the increase in porosity and the formation of terminal silanol groups on the newly developed pore surface after the desilication treatment. Thus, combining the coating of zeolite crystals on the surface of diatomite with a controlled desilication by an optimal desilication treatment may allow for a new approach in the preparation of promising benzene adsorbents.

Acknowledgments

The work was supported by the Team Project of Natural Science Foundation of Guangdong Province, China (Grant No. S2013030014241), National Key Technology Research and Development Program of the Ministry of Science and Technology of China (Grant No. 2013BAC01B02), National Natural Science Foundation of China (Grant No. 41202024), and the Science and Technology Program of Guangzhou, China. This is a contribution (NO. IS-2039) from GIGCAS.

Appendix A. Supplementary data

Supplementary data associated with this article can be found, in the online version, at http://dx.doi.org/10.1016/j.cej.2015.02.065.

References

[1] H. Einaga, S. Futamura, T. Ibusuki, Complete oxidation of benzene in gas phase by platinized titania photocatalysts, Environ. Sci. Technol. 35 (2001) 1880–1884.
[2] D.P. Serrano, G. Calleja, J.A. Botas, F.J. Gutierrez, Adsorption and hydrophobic properties of mesostructured MCM-41 and SBA-15 materials for volatile organic compound removal, Ind. Eng. Chem. Res. 43 (2004) 7010–7018.
[3] Q. Hu, J.J. Li, Z.P. Hao, L.D. Li, S.Z. Qiao, Dynamic adsorption of volatile organic compounds on organofunctionalized SBA-15 materials, Chem. Eng. J. 149 (2009) 281–288.
[4] P. Dwivedi, V. Gaur, A. Sharma, N. Verma, Comparative study of removal of volatile organic compounds by cryogenic condensation and adsorption by activated carbon fiber, Sep. Purif. Technol. 39 (2004) 23–37.
[5] S. Liu, W. Teo, X. Tan, K. Li, Preparation of $PDMS^{vi}$–Al_2O_3 composite hollow fibre membranes for VOC recovery from waste gas streams, Sep. Purif. Technol. 46 (2005) 110–117.
[6] S. Azalim, R. Brahmi, M. Agunaou, A. Beaurain, J.M. Giraudon, J.F. Lamonier, Washcoating of cordierite honeycomb with Ce–Zr–Mn mixed oxides for VOC catalytic oxidation, Chem. Eng. J. 223 (2013) 536–546.
[7] A. Changsuphan, M.I.B.A. Wahab, N.T. Kim Oanh, Removal of benzene by ZnO nanoparticles coated on porous adsorbents in presence of ozone and UV, Chem. Eng. J. 181–182 (2012) 215–221.
[8] L. Li, S. Wang, Q. Feng, J. Liu, Removal of o-xylene from off-gas by a combination of bioreactor and adsorption, Asia-Pac. J. Chem. Eng. 3 (2008) 489–496.
[9] H. Wang, M. Tang, K. Zhang, D. Cai, W. Huang, R. Chen, C. Yu, Functionalized hollow siliceous spheres for VOCs removal with high efficiency and stability, J. Hazard. Mater. 268 (2014) 115–123.
[10] N. Mohan, G. Kannan, S. Upendra, R. Subha, N. Kumar, Breakthrough of toluene vapours in granular activated carbon filled packed bed reactor, J. Hazard. Mater. 168 (2009) 777–781.
[11] X. Zhao, Q. Ma, G. Lu, VOC removal: comparison of MCM-41 with hydrophobic zeolites and activated carbon, Energy Fuels 12 (1998) 1051–1054.
[12] P. Huttenloch, K.E. Roehl, K. Czurda, Sorption of nonpolar aromatic contaminants by chlorosilane surface modified natural minerals, Environ. Sci. Technol. 35 (2001) 4260–4264.
[13] Y. Bai, Z.-H. Huang, F. Kang, Synthesis of reduced graphene oxide/phenolic resin-based carbon composite ultrafine fibers and their adsorption performance for volatile organic compounds and water, J. Mater. Chem. A 1 (2013) 9536–9543.
[14] H. Wang, M. Tang, L. Han, J. Cao, Z. Zhang, W. Huang, R. Chen, C. Yu, Synthesis of hollow organosiliceous spheres for volatile organic compound removal, J. Mater. Chem. A 2 (2014) 19298–19307.
[15] Z. Zhao, S. Wang, Y. Yang, X. Li, J. Li, Z. Li, Competitive adsorption and selectivity of benzene and water vapor on the microporous metal organic frameworks (HKUST-1), Chem. Eng. J. 259 (2015) 79–89.
[16] D. Olson, G. Kokotailo, S. Lawton, W. Meier, Crystal structure and structure-related properties of ZSM-5, J. Phys. Chem. 85 (1981) 2238–2243.
[17] K. Zhang, R.P. Lively, J.D. Noel, M.E. Dose, B.A. McCool, R.R. Chance, W.J. Koros, Adsorption of water and ethanol in MFI-type zeolites, Langmuir 28 (2012) 8664–8673.
[18] G. Xomeritakis, M. Tsapatsis, Permeation of aromatic isomer vapors through oriented MFI-type membranes made by secondary growth, Chem. Mater. 11 (1999) 875–878.
[19] J. Zhang, Q. Ping, M. Niu, H. Shi, N. Li, Kinetics and equilibrium studies from the methylene blue adsorption on diatomite treated with sodium hydroxide, Appl. Clay Sci. 83 (2013) 12–16.
[20] H. Alijani, M.H. Beyki, Z. Shariatinia, M. Bayat, F. Shemirani, A new approach for one step synthesis of magnetic carbon nanotubes/diatomite earth composite by chemical vapor deposition method: application for removal of lead ions, Chem. Eng. J. 253 (2014) 456–463.
[21] P. Yuan, D. Liu, M.D. Fan, D. Yang, R.L. Zhu, F. Ge, J.X. Zhu, H.P. He, Removal of hexavalent chromium [Cr(VI)] from aqueous solutions by the diatomite-supported/unsupported magnetite nanoparticles, J. Hazard. Mater. 173 (2010) 614–621.
[22] N. van Garderen, F.J. Clemens, M. Mezzomo, C.P. Bergmann, T. Graule, Investigation of clay content and sintering temperature on attrition resistance of highly porous diatomite based material, Appl. Clay Sci. 52 (2011) 115–121.
[23] P. Yuan, D. Liu, D.Y. Tan, K.K. Liu, H.G. Yu, Y.H. Zhong, A.H. Yuan, W.B. Yu, H.P. He, Surface silylation of mesoporous/macroporous diatomite (diatomaceous earth) and its function in Cu (II) adsorption: the effects of heating pretreatment, Microporous Mesoporous Mater. 170 (2013) 9–19.
[24] J. Jin, J. Ouyang, H. Yang, One-step synthesis of highly ordered Pt/MCM-41 from natural diatomite and the superior capacity in hydrogen storage, Appl. Clay Sci. 99 (2014) 246–253.
[25] M.W. Anderson, S.M. Holmes, N. Hanif, C.S. Cundy, Hierarchical pore structures through diatom zeolitization, Angew. Chem. Int. Ed. 39 (2000) 2707–2710.
[26] Y.J. Wang, Y. Tang, A.G. Dong, X.D. Wang, N. Ren, Z. Gao, Zeolitization of diatomite to prepare hierarchical porous zeolite materials through a vapor-phase transport process, J. Mater. Chem. 12 (2002) 1812–1818.
[27] H. Liu, G. Lu, Y. Guo, Y. Guo, J. Wang, Deactivation and regeneration of TS-1/diatomite catalyst for hydroxylation of phenol in fixed-bed reactor, Chem. Eng. J. 108 (2005) 187–192.
[28] J. Van Bokhoven, M. Tromp, D. Koningsberger, J. Miller, J. Pieterse, J. Lercher, B. Williams, H. Kung, An explanation for the enhanced activity for light alkane conversion in mildly steam dealuminated mordenite: the dominant role of adsorption, J. Catal. 202 (2001) 129–140.
[29] S. Van Donk, A.H. Janssen, J.H. Bitter, K.P. de Jong, Generation, characterization, and impact of mesopores in zeolite catalysts, Catal. Rev. 45 (2003) 297–319.
[30] J. Groen, L. Peffer, J. Moulijn, J. Pérez-Ramırez, Mesoporosity development in ZSM-5 zeolite upon optimized desilication conditions in alkaline medium, Colloids Surf. A 241 (2004) 53–58.
[31] J. Pérez-Ramırez, F. Kapteijn, J.C. Groen, A. Doménech, G. Mul, J.A. Moulijn, Steam-activated FeMFI zeolites. Evolution of iron species and activity in direct N_2O decomposition, J. Catal. 214 (2003) 33–45.
[32] J.C. Groen, J.A. Moulijn, J. Perez-Ramirez, Desilication: on the controlled generation of mesoporosity in MFI zeolites, J. Mater. Chem. 16 (2006) 2121–2131.
[33] J.C. Groen, W. Zhu, S. Brouwer, S.J. Huynink, F. Kapteijn, J.A. Moulijn, J. Pérez-Ramírez, Direct demonstration of enhanced diffusion in mesoporous ZSM-5 zeolite obtained via controlled desilication, J. Am. Chem. Soc. 129 (2007) 355–360.
[34] S.M. Holmes, C. Markert, R.J. Plaisted, J.O. Forrest, J.R. Agger, M.W. Anderson, C.S. Cundy, J. Dwyer, A novel method for the growth of silicalite membranes on stainless steel supports, Chem. Mater. 11 (1999) 3329–3332.
[35] B. Louis, F. Ocampo, H.S. Yun, J.P. Tessonnier, M.M. Pereira, Hierarchical pore ZSM-5 zeolite structures: from micro- to macro-engineering of structured catalysts, Chem. Eng. J. 161 (2010) 397–402.

[36] M.V. Twigg, J.T. Richardson, Fundamentals and applications of structured ceramic foam catalysts, Ind. Eng. Chem. Res. 46 (2007) 4166–4177.
[37] P. Yuan, D. Yang, Z.Y. Lin, H.P. He, X.Y. Wen, L.J. Wang, F. Deng, Influences of pretreatment temperature on the surface silylation of diatomaceous amorphous silica with trimethylchlorosilane, J. Non-Cryst. Solids 352 (2006) 3762–3771.
[38] A.E. Persson, B.J. Schoeman, J. Sterte, J.E. Otterstedt, The synthesis of discrete colloidal particles of TPA-silicalite-1, Zeolites 14 (1994) 557–567.
[39] Y. Wang, Y. Tang, X. Wang, A. Dong, W. Shan, Z. Gao, Fabrication of hierarchically structured zeolites through layer-by-layer assembly of zeolite nanocrystals on diatom templates, Chem. Lett. 30 (2001) 1118–1119.
[40] S. Brunauer, P.H. Emmett, E. Teller, Adsorption of gases in multimolecular layers, J. Am. Chem. Soc. 60 (1938) 309–319.
[41] B.C. Lippens, J. De Boer, Studies on pore systems in catalysts: V. The t method, J. Catal. 4 (1965) 319–323.
[42] E.P. Barrett, L.G. Joyner, P.P. Halenda, The determination of pore volume and area distributions in porous substances. I. Computations from nitrogen isotherms, J. Am. Chem. Soc. 73 (1951) 373–380.
[43] A. Saito, H.C. Foley, Argon porosimetry of selected molecular sieves: experiments and examination of the adapted Horvath-Kawazoe model, Microporous Mater. 3 (1995) 531–542.
[44] B. Dou, J. Li, Y. Wang, H. Wang, C. Ma, Z. Hao, Adsorption and desorption performance of benzene over hierarchically structured carbon–silica aerogel composites, J. Hazard. Mater. 196 (2011) 194–200.
[45] Á. Berenguer-Murcia, A.J. Fletcher, J. García-Martínez, D. Cazorla-Amoros, Á. Linares-Solano, K.M. Thomas, Probe molecule kinetic studies of adsorption on MCM-41, J. Phys. Chem. B 107 (2003) 1012–1020.
[46] B.T. Holland, L. Abrams, A. Stein, Dual templating of macroporous silicates with zeolitic microporous frameworks, J. Am. Chem. Soc. 121 (1999) 4308–4309.
[47] S. Gregg, K.S.W. Sing, Surface Area and Porosity, Academic Press Inc., Ltd., London, 1982.
[48] P. Yuan, M.D. Fan, D. Yang, H.P. He, D. Liu, A.H. Yuan, J.X. Zhua, T.H. Chen, Montmorillonite-supported magnetite nanoparticles for the removal of hexavalent chromium Cr(VI) from aqueous solutions, J. Hazard. Mater. 166 (2009) 821–829.
[49] D. Liu, P. Yuan, D. Tan, H. Liu, T. Wang, M. Fan, J. Zhu, H. He, Facile preparation of hierarchically porous carbon using diatomite as both template and catalyst and methylene blue adsorption of carbon products, J. Colloid Interface Sci. 388 (2012) 176–184.
[50] S. Lopez-Orozco, A. Inayat, A. Schwab, T. Selvam, W. Schwieger, Zeolitic materials with hierarchical porous structures, Adv. Mater. 23 (2011) 2602–2615.
[51] R. Le Van Mao, S. Le, D. Ohayon, F. Caillibot, L. Gelebart, G. Denes, Modification of the micropore characteristics of the desilicated ZSM-5 zeolite by thermal treatment, Zeolites 19 (1997) 270–278.
[52] Y. Wong, Y. Szeto, W. Cheung, G. McKay, Equilibrium studies for acid dye adsorption onto chitosan, Langmuir 19 (2003) 7888–7894.
[53] X. Lin, A.J. Blake, C. Wilson, X.Z. Sun, N.R. Champness, M.W. George, P. Hubberstey, R. Mokaya, M. Schroder, A porous framework polymer based on a zinc(II) 4,4′-bipyridine-2,6,2′,6′-tetracarboxylate: synthesis, structure, and "zeolite-like" behaviors, J. Am. Chem. Soc. 128 (2006) 10745–10753.
[54] B.J. Dou, J.J. Li, Q. Hu, C.Y. Ma, C. He, P. Li, Q.H. Hu, Z.P. Hao, S.Z. Qiao, Hydrophobic micro/mesoporous silica spheres assembled from zeolite precursors in acidic media for aromatics adsorption, Microporous Mesoporous Mater. 133 (2010) 115–123.
[55] T. Armaroli, M. Trombetta, A.G. Alejandre, J.R. Solis, FTIR study of the interaction of some branched aliphatic molecules with the external and internal sites of H-ZSM5 zeolite, Phys. Chem. Chem. Phys. 2 (2000) 3341–3348.
[56] P.A. Jacobs, J.A. Martens, J. Weitkamp, H.K. Beyer, Shape-selectivity changes in high-silica zeolites, Faraday Discuss. Chem. Soc. 72 (1981) 353–369.
[57] E.M. Flanigen, J. Bennett, R. Grose, J. Cohen, R. Patton, R. Kirchner, Silicalite, a new hydrophobic crystalline silica molecular sieve, Nature 271 (1978) 512–516.
[58] G. Dosseh, Y. Xia, C. Alba-Simionesco, Cyclohexane and benzene confined in MCM-41 and SBA-15: confinement effects on freezing and melting, J. Phys. Chem. B 107 (2003) 6445–6453.
[59] K. Kosuge, S. Kubo, N. Kikukawa, M. Takemori, Effect of pore structure in mesoporous silicas on VOC dynamic adsorption/desorption performance, Langmuir 23 (2007) 3095–3102.
[60] A.J. Fletcher, Y. Yuzak, K.M. Thomas, Adsorption and desorption kinetics for hydrophilic and hydrophobic vapors on activated carbon, Carbon 44 (2006) 989–1004.
[61] L.J. Song, Z.L. Sun, H.Y. Ban, M. Dai, L.V.C. Rees, Studies of unusual adsorption and diffusion behaviour of benzene in silicalite-1, Phys. Chem. Chem. Phys. 6 (2004) 4722–4731.